Hierarchical Coordination Optimization Method of Isolated Electricity-hydrogen Microgrids with High Penetration of Renewable Energy Sources

Jizhong Zhu, Taiheng Guo, Shenglin Li, Hanjiang Dong, Alberto Borghetti, and Xuemeng Lan

***Abstract*—Renewable energy sources (RESs), particularly solar and wind energy, present a viable pathway for decarbonizing isolated microgrids (MGs). However, as the penetration of RESs increases, ensuring the optimal utilization of RESs while maintaining the system reliability poses significant challenges for isolated MGs. Therefore, a hierarchical coordination optimization method of the isolated electricity-hydrogen MG with high penetration of RESs is proposed to achieve low-carbon dispatching. The developed isolated electricity-hydrogen MG is an integrated system featuring hybrid battery-hydrogen energy storage, which encompasses three interconnected subsystems: an AC subsystem, a DC subsystem, and a hydrogen subsystem. The proposed method can be divided into two dispatch horizons: an annual horizon and a daily horizon. The annual horizon focuses on the inter-day energy dispatch, addressing hydrogen storage boundary conditions to solve seasonal energy mismatches. The daily horizon focuses on the day-ahead power dispatch to ensure the daily power balance of MG, taking into account the errors in annual estimated data. The effectiveness of the proposed method is validated through a series of case studies for an isolated electricity-hydrogen MG under varying penetrations of RESs and energy storage configurations. Simulation results show the promising potential of the proposed method in facilitating sustainable isolated electricity-hydrogen MGs.**

***Index Terms*—Microgrid (MG), renewable energy source (RES), hybrid battery-hydrogen energy storage, energy management system.**

Manuscript received: April 5, 2025; revised: June 30, 2025; accepted: August 18, 2025. Date of CrossCheck: August 18, 2025. Date of online publication: November 12, 2025.

This work was supported by the Guangdong Basic and Applied Basic Research Foundation (No. 2023A1515110195), the Postdoctoral Fellowship Program of CPSF (No. GZC20230834), and the National Natural Science Foundation of China (No. 52177087).

J. Zhu, S. Li (corresponding author), H. Dong, and X. Lan are with the School of Electric Power Engineering, South China University of Technology, Guangzhou 510640, China (e-mail: zhujz@scut.edu.cn; iamlshl@scut.edu.cn; hanjiang.dong@foxmail.com; 2498306255@qq.com).

T. Guo is with the Electric Power Research Institute of Guangdong Power Grid Co., Ltd., Guangzhou 510080, China, and he is also with the School of Electric Power Engineering, South China University of Technology, Guangzhou 510640, China (e-mail: epguoth@163.com).

A. Borghetti is with the Department of Electrical, Electronic and Information Engineering, University of Bologna, Bologna 40136, Italy (e-mail: alberto.borghetti@unibo.it).

DOI: 10.35833/MPCE.2025.000303

NOMENCLATURE

A. Indices and Sets

ε_N, ε_M	Branch sets of AC and DC networks
d, D	Index and number of days
j	Index of nodes
N, M	Node sets of AC and DC networks
t, T	Index and number of time intervals in a day
Δt, Δd	Time resolutions of day-ahead power dispatch and inter-day energy dispatch

B. Parameters

$\eta_{BC,D2A}$	Conversion efficiency of DC to AC (D2A) via bidirectional converter (BC) (%)
$\eta_{BC,A2D}$	Conversion efficiency AC to DC (A2D) via BC (%)
η_{ED}, η_{HFC}	Efficiencies of electrolyzer device (ED) and hydrogen fuel cell (HFC) (%)
$\eta_{H,ch}$, $\eta_{H,dch}$	Charging and discharging efficiencies of hydrogen energy storage (HES) (%)
$\eta_{B,ch}$, $\eta_{B,dch}$	Charging and discharging efficiencies of battery energy storage (BES) (%)
$\eta_{B,self}$, $\eta_{H,self}$	Self-discharging rates of BES (%/h) and HES (%/day)
π_C, c_G	Carbon tax ($/kg) and diesel engine (DE) emission coefficient (kg/L)
ζ_H^d	End-of-day state-of-hydrogen (SOH) considering deviation
$\varepsilon_{SOH,max}$	Correction threshold of SOH
γ_{AL}	Power factor angle (rad)
a_{DE}, b_{DE}	Fit coefficients of daily cost of DE
$C_{ap,H}$, $C_{ap,B}$	Total energy capacities of HES (kg) and BES (kWh)
$D_{min}^{off,\Delta t}$	The minimum continuous shutdown duration of DE (hour)
$D_{min}^{on,\Delta t}$, $D_{max}^{on,\Delta t}$	The minimum and maximum continuous operating durations of DE (hour)
E_{WTG}^d, E_{PVG}^d	Electricity generation of wind turbine (WT) and photovoltaic (PV) (kWh)

$E_{\mathrm{AL,A}}^{d}$, $E_{\mathrm{DL,A}}^{d}$ Critical AC and DC load demands (kWh)

$E_{\mathrm{AL,A\&B}}^{d}$, $E_{\mathrm{DL,A\&B}}^{d}$ The maximum AC and DC load demands (kWh)

$E_{\mathrm{HL,A}}^{d}$, $E_{\mathrm{HL,A\&B}}^{d}$ Critical and the maximum hydrogen load demands (kg)

$E_{\mathrm{DE,min}}^{d}$, $E_{\mathrm{DE,max}}^{d}$ The minimum and maximum output electricity of DE (kWh)

$\Delta E_{\mathrm{ED}}^{d}$ Energy deviation of ED (kWh)

$\Delta E_{\mathrm{HFC}}^{d}$ Energy deviation of HFC (kWh)

$\Delta E_{\mathrm{H,ch}}^{d}$, $\Delta E_{\mathrm{H,dch}}^{d}$ Energy deviations of charging and discharging hydrogen of HES (kg)

$\Delta E_{\mathrm{BC,A2B}}^{d}$ Energy deviation of AC bus to BC (A2B) (kWh)

$\Delta E_{\mathrm{BC,B2A}}^{d}$ Energy deviation of BC to AC bus (B2A) (kWh)

$\Delta E_{\mathrm{AC,NG}}^{d}$ Net generation deviation of AC subsystem (kWh)

$\Delta E_{\mathrm{DC,NG}}^{d}$ Net generation deviation of DC subsystem (kWh)

$\Delta E_{\mathrm{H,NG}}^{d}$ Net generation deviation of hydrogen subsystem (kg)

$error_{\mathrm{WT}}^{d}$ Estimation error of annual WT generation (kWh)

$error_{\mathrm{PV}}^{d}$ Estimation error of annual PV generation (kWh)

$error_{\mathrm{AL}}^{d}$ Estimation error of annual AC load (kWh)

$error_{\mathrm{DL}}^{d}$ Estimation error of annual DC load (kWh)

$error_{\mathrm{HL}}^{d}$ Estimation error of annual hydrogen load (kg)

F_1, F_2 Fuel consumption coefficients of DE

$G_{\mathrm{HL,A}}^{t}$, $G_{\mathrm{HL,A\&B}}^{t}$ Critical and the maximum hydrogen load demands (kg/h)

$G_{\mathrm{H,ch,max}}$, $G_{\mathrm{H,dch,max}}$ The maximum charging and discharging hydrogen of HES (kg/h)

$m_{\mathrm{H}}^{\mathrm{O\&M}}$, $m_{\mathrm{BC}}^{\mathrm{O\&M}}$, $m_{\mathrm{ED}}^{\mathrm{O\&M}}$, $m_{\mathrm{HFC}}^{\mathrm{O\&M}}$, $m_{\mathrm{B}}^{\mathrm{O\&M}}$, $m_{\mathrm{DE}}^{\mathrm{O\&M}}$, $m_{\mathrm{PV}}^{\mathrm{O\&M}}$, $m_{\mathrm{WT}}^{\mathrm{O\&M}}$ Operation and maintenance (O&M) prices of HES ($/kg), BC, ED, HFC, BES, DE, PV, and WT ($/kWh)

$m_{\mathrm{EL}}^{\mathrm{cur}}$, $m_{\mathrm{HL}}^{\mathrm{cur}}$ Prices of electric ($/kWh) and hydrogen ($/kg) load curtailments

$m_{\mathrm{B}}^{\mathrm{dep}}$, $m_{\mathrm{HFC}}^{\mathrm{dep}}$, $m_{\mathrm{ED}}^{\mathrm{dep}}$ Depreciation prices of BES, HFC, and ED ($/kWh)

$m_{\mathrm{H}}^{\mathrm{dep}}$ Depreciation price of HES ($/kg)

P_{WTG}^{t}, P_{PVG}^{t} Active power generated by WT and PV (kW)

$P_{\mathrm{AL,A}}^{t}$, $P_{\mathrm{DL,A}}^{t}$ Critical active power of AC and DC loads (kW)

$P_{\mathrm{AL,A\&B}}^{t}$, $P_{\mathrm{DL,A\&B}}^{t}$ The maximum active power of AC and DC loads (kW)

$P_{\mathrm{D2B,max}}$, The maximum active power of DC bus to BC (D2B) and A2B (kW)

$P_{\mathrm{ED,min}}$, $P_{\mathrm{ED,max}}$ The minimum and maximum active power of ED (kW)

$P_{\mathrm{HFC,min}}$, $P_{\mathrm{HFC,max}}$ The minimum and maximum active power of HFC (kW)

$P_{\mathrm{DE,min}}$, $P_{\mathrm{DE,max}}$ The minimum and maximum active power of DE (kW)

$P_{\mathrm{B,ch,max}}$, $P_{\mathrm{B,dch,max}}$ The maximum charging and discharging power of BES (kW)

$P_{ij,\mathrm{DC,max}}$ The maximum active power of branch (kW)

$P_{\mathrm{DE,r}}$ Rated power capacity of DE (kW)

$\Delta P_{\mathrm{BC,dw}}^{\Delta t}$, $\Delta P_{\mathrm{BC,up}}^{\Delta t}$ The maximum ramp down and up power of BC (kW/h)

$\Delta P_{\mathrm{ED,dw}}^{\Delta t}$, $\Delta P_{\mathrm{ED,up}}^{\Delta t}$ The maximum ramp down and up power of ED (kW/h)

$\Delta P_{\mathrm{HFC,dw}}^{\Delta t}$, $\Delta P_{\mathrm{HFC,up}}^{\Delta t}$ The maximum ramp down and up power of HFC (kW/h)

$\Delta P_{\mathrm{DE,dw}}^{\Delta t}$, $\Delta P_{\mathrm{DE,up}}^{\Delta t}$ The maximum ramp down and up power of DE (kW/h)

r_{ij}, x_{ij} Resistance and reactance of branch

$S_{\mathrm{H,min}}$, $S_{\mathrm{H,max}}$ The minimum and maximum SOHs of HES

$S_{\mathrm{B,min}}$, $S_{\mathrm{B,max}}$ The minimum and maximum states-of-charge (SOCs) of BES

$S_{\mathrm{H}}^{\mathrm{ini}}$, $S_{\mathrm{B}}^{\mathrm{ini}}$ The initial SOH of HES and SOC of BES

S_{BC}, S_{DE}, S_{WT} Capacities of BC, DE, and WT (kVA)

$S_{ij,\mathrm{AC,max}}$ The maximum apparent power of branch (kVA)

$S_{\mathrm{H,new}}^{d}$ Corrected SOH at the end of day

$\Delta S_{\mathrm{H,error}}^{d}$ SOH deviation of HES caused by estimation error

V_{HHV} Higher heating value of hydrogen (MJ/kg)

$V_{\mathrm{DE}}^{\mathrm{start}}$, $V_{\mathrm{DE}}^{\mathrm{fuel}}$ Start-up price ($) and fuel price ($/L) of DE

$v_{\min}$, $v_{\max}$ The minimum and maximum values of square voltage

C. Variables

E_{A2B}^{d}, E_{D2B}^{d} Electricity of A2B and D2B (kWh)

$E_{\mathrm{ED,in}}^{d}$, $E_{\mathrm{ED,out}}^{d}$ Input electricity (kWh) and output hydrogen (kg) of ED

$E_{\mathrm{HFC,in}}^{d}$, $E_{\mathrm{HFC,out}}^{d}$ Input hydrogen (kg) and output electricity (kWh) of HFC

E_{WT}^{d}, E_{PV}^{d}, E_{DE}^{d} Electricity of WT, PV, and DE for dispatch (kWh)

E_{AL}^{d}, E_{DL}^{d}, E_{HL}^{d} AC (kWh), DC (kWh), and hydrogen load demands (kg)

$E_{\mathrm{H,ch}}^{d}$, $E_{\mathrm{H,dch}}^{d}$ Charging and discharging hydrogen of HES (kg)

F_{fuel}^{t} Fuel consumption rate of DE (L/h)

G_{AL}^{t} Reactive power of AC load (kvar)

$G_{\mathrm{HL,cur}}^{t}$ Hydrogen load curtailment (kg/h)

G_{HFC}^{t}, G_{ED}^{t} Hydrogen inflow/outflow of HFC and ED (kg/h)

$G_{\mathrm{H,ch}}^{t}$, $G_{\mathrm{H,dch}}^{t}$ Charging and discharging hydrogen of HES (kg/h)

G_{HL}^{t} Hydrogen load demand (kg/h)

l_{ij}^{t} Square current of branch

$P_{\mathrm{AC}}^{t,j}$, $Q_{\mathrm{AC}}^{t,j}$ Active power (kW) and reactive power (kvar) in AC subsystem

$P_{\mathrm{DC}}^{t,j}$ Active power in DC subsystem (kW)

P_{ij}^{t}, Q_{ij}^{t}	Active power (kW) and reactive power (kvar) of branch
$P_{\mathrm{WT}}^{t,j}$, $P_{\mathrm{PV}}^{t,j}$, $P_{\mathrm{DE}}^{t,j}$	Active power of WT, PV, and DE for dispatch (kW)
P_{HFC}^{t}, P_{ED}^{t}	Output/input active power of HFC and ED (kW)
P_{AL}^{t}, P_{DL}^{t}, G_{HL}^{t}	Active power of AC load (kW), DC load (kW), and hydrogen load (kg/h)
$P_{\mathrm{AL,cur}}^{t,j}$, $P_{\mathrm{DL,cur}}^{t,j}$	Active power of AC and DC load curtailments (kW)
$P_{\mathrm{B,ch}}^{t,j}$, $P_{\mathrm{B,dch}}^{t,j}$	Charging and discharging active power of BES (kW)
$P_{\mathrm{B2A}}^{t,j}$, $P_{\mathrm{B2D}}^{t,j,}$	Active power of B2A and BC to DC bus (B2D) (kW)
$P_{\mathrm{A2B}}^{t,j}$, $P_{\mathrm{D2B}}^{t,j}$	Active power of A2B and D2B (kW)
$Q_{\mathrm{BC}}^{t,j}$, $Q_{\mathrm{DE}}^{t,j}$, $Q_{\mathrm{WT}}^{t,j}$	Reactive power of BC, DE, and WT (kvar)
$Q_{\mathrm{WT}}^{t,j}$, $Q_{\mathrm{PV}}^{t,j}$, $Q_{\mathrm{DE}}^{t,j}$	Reactive power of WT, PV, and DE for dispatch (kvar)
$Q_{\mathrm{AL}}^{t,j}$	Reactive power of AC load (kvar)
S_{H}^{t}, S_{B}^{t}	SOH of HES and SOC of BES
u_{BC}^{t}	State of BC in daily horizon (1 for D2B and 0 for A2B)
u_{ED}^{t}, u_{HFC}^{t}, u_{DE}^{t}	States of ED, HFC, and DE in daily horizon (1 for working)
u_{B}^{t}, u_{H}^{t}	States of BES and HES in daily horizon (1 for charging)
u_{BC}^{d}	State of BC in annual horizon (1 for D2B and 0 for A2B)
u_{ED}^{d}, u_{HFC}^{d}, u_{DE}^{d}	States of ED, HFC, and DE in annual horizon (1 for working)
u_{H}^{d}	State of HES in annual horizon (1 for charging)
$v^{t,j}$	Squared voltage at node

I. Introduction

To achieve the purpose of greenhouse gas emission reduction, the development of renewable energy sources (RESs) is crucial [1]. The International Energy Agency (IEA) reports that RESs may become the dominant energy source to achieve net zero [2]. In 2021, the wind and solar share climbed above 10% of world electricity generation [3]. However, the power output of solar and wind energy has a stochastic and intermittent nature [4], [5]. These intrinsic features impose difficulties and challenges on microgrid (MG) operation, which is the bottleneck problem restricting the application of high penetration of RESs.

Diesel generators are frequently employed as primary power sources in isolated MGs to ensure the reliability of power supply. Expensive electricity and polluting gas emissions are two features of isolated MGs [6]. Therefore, enhancing environmental friendliness and ensuring supply reliability are two critical issues that require urgent attention for isolated MGs. In order to achieve the MG decarbonization, some controllable power sources such as diesel generators will gradually be replaced by uncontrollable RESs. Consequently, the operation mode of isolated MGs with a high penetration of RESs will shift from power source adjustment to coordinating among sources, loads, and storage facilities.

The deployment of energy storage system (ESS) is one of the practical and efficient measures to promote the consumption of RESs and reliable operation [7]. The energy storage sector has experienced significant growth in recent years. According to the latest industry report from China Energy Storage Alliance (CNESA), by the end of 2022, the total electricity storage capacity in operation worldwide had reached 237.2 GW [8]. Lithium-ion batteries are growing the fastest as a representative of electrochemical energy storage. Noted that pumped hydro storage is highly dependent on geographical conditions, and it is generally unsuitable for small- and medium-scale MGs.

Battery energy storage (BES) is typically utilized for short-term energy storage to participate in daily cycling applications such as power balancing, peak shaving, and frequency regulation [9]. A hybrid battery/ultracapacitor ESS is proposed in [10] to meet the requirements of the highly-dynamic current demands and steady-state loads. The analysis of a campus MG indicated that the excessive integration of RESs would result in excess power, necessitating a large-scale ESS [11]. In contrast, BES is not suitable for long-term and large-scale energy storage due to its low energy density and non-negligible self-discharging rate. The long-term energy storage is employed to address the seasonal energy mismatch between RES supply and electricity demand in decarbonized power systems [12]. The study in [13] suggested that a hydrogen energy storage (HES) system could be significantly deployed as a long-term and large-scale energy storage solution because of its decoupling of energy capacity from power capacity. However, the low conversion efficiencies, high investment costs, and security concerns remain the primary barriers to the widespread application of HES. Recently, the emphasis on environmental protection has made HES more competitive [14]. Additionally, HES offers unique benefits in isolated MGs, as most isolated MGs typically depend on fossil fuel-based electricity [15]. This paper achieves the coordinated long-term and short-term operations of isolated MGs with RESs by using a hybrid battery-hydrogen ESS.

Regarding the consumption of high penetration of RESs, most existing research has focused on energy system planning and operation. In [16], an optimal planning model based on a two-stage full-data processing approach is proposed for MGs with RESs, in which the two timescales with different resolutions are included. Reference [17] presents a multistage stochastic optimization model for the power distribution system and hydrogen energy system, optimizing the investment decisions on network assets, capacities of power to hydrogen (P2H) and hydrogen storage, ultimately reducing planning costs and promoting renewable energy consumption. The work in [18] proposes a novel energy-sharing mechanism for smart MGs with RESs and ESSs to achieve the energy source sharing and trading. However, these studies have given limited consideration to the integration of hydrogen technologies in decarbonized MGs, and the impact of long-term and large-scale energy storage on seasonal energy balance has not been fully addressed.

In recent years, the hydrogen energy has been integrated into power systems to address the spatiotemporal imbalance between RES generation and hydrogen demand [19] and to enhance the RES accommodation [20]. Reference [20] developed a day-ahead economic dispatch for a grid-connected electrical-gas-hydrogen MG. However, this work heavily depended on the main grid and ignored environmental factors. To improve the RES utilization, [21] presented reasonable power to heat and P2H as well as HES models for an integrated energy system with ultra-high penetration of RESs. Reference [22] proposed a multistage stochastic mixed-integer programming approach to optimize the synergy between seasonal and short-term energy storage in hydrogen-enabled multi-energy MGs. These studies verified that the hydrogen energy holds significant potential to boost RES accommodation and facilitate system decarbonization. However, the operational strategies are not applicable to isolated MGs, as they cannot use the main grid as an energy supplement to maintain energy balance. Hence, the decarbonization of isolated MGs is more challenging than that of grid-connected MGs.

The research on energy management systems (EMSs) considering multi-time-scale coordination has been extensively studied. Predicted errors are inevitable due to uncertainties, particularly in MGs with high penetration of RESs [23]. For example, to compensate for source-load deviations in islanded hybrid AC/DC MGs, [24] proposes a multi-time-scale rolling optimization method, which includes a day-ahead scale, a short-term scale, and a real-time scale. In [25], a three-level hierarchical coordination method including top, medium, and bottom levels is proposed for MGs to address supply-demand imbalances, which also considers energy trading among different MGs. A multi-time-scale hierarchical control strategy is also developed for the Dongao Island MG, China, solving the frequency stability problem [26]. Reference [27] presents a two-layer EMS for MGs, where the two layers focus on minimizing operational costs and eliminating power fluctuations, respectively. In [28], a dynamic and precise operating reserve scheme is developed within the multi-time-scale EMS to accurately allocate BES capacity for economic scheduling and operating reserve. MGs with a small or medium share of RESs are flexible enough to avoid seasonal energy mismatches. To advance the decarbonization, it is necessary to increase the percentage of RESs and deploy the long-term ESSs. Further research efforts are needed for the development of optimization methods for isolated MGs, considering annual and daily timescales within the context of decarbonization.

Isolated MGs with high penetration of RESs face a dual challenge of daily power intermittency and seasonal energy mismatches. As the penetration of RESs increases, the issues of power curtailment and supply reliability are expected to worsen. These are also new challenges for traditional MGs and conventional dispatch methods. Therefore, this paper proposes a hierarchical coordination optimization method of isolated electricity-hydrogen MGs with high penetration of RESs. The main contributions of this paper can be summarized as follows.

1) To achieve the decarbonized isolated MGs, an isolated electricity-hydrogen MG with high penetration of RESs is considered. This paper constructs an isolated electricity-hydrogen MG consisting of an AC subsystem, a DC subsystem, and a hydrogen subsystem. Moreover, a hybrid ESS with BES and HES is proposed to ensure the reliability of both long-term and short-term power.

2) The proposed method employs two dispatch horizons to realize the coordination operation of isolated electricity-hydrogen MGs under high and super-high penetrations of RESs. In the proposed method, the annual horizon is dedicated to solving seasonal energy mismatches, while the daily horizon focuses on achieving daily power balance. The prediction errors and carbon emission costs are also taken into account.

3) Currently, due to the significant error, it is generally inaccurate to forecast energy data a year in advance. We utilize the spare capacity of HES to mitigate the deviation of renewable energy output and load demand from annual estimated data. It aims to increase the utilization of hydrogen storage and guarantee the reliable and economic operation of isolated electricity-hydrogen MGs.

The remainder of this paper is organized as follows. The isolated electricity-hydrogen MG modeling is presented in Section II. Section III formulates the dispatch problem. Simulation results are presented and discussed in Section IV. Finally, Section V summarizes the conclusion and identifies the areas that need a further research effort.

II. Isolated Electricity-hydrogen MG Modeling

A. System Architecture

The system architecture of the isolated electricity-hydrogen MG is shown in Fig. 1. Currently, a considerable share of power generation resources in MGs produces DC power, and a growing number of electric devices operate on DC bus. On one hand, connecting these generation resources and DC loads to a DC MG with the appropriate voltage may significantly minimize the losses and costs associated with power electronic equipment. On the other hand, hydrogen is a large-scale and low-carbon energy storage medium that plays a key role of energy balancing in MGs with high penetration of RESs. Therefore, the isolated electricity-hydrogen MG is divided into three energy subsystems: AC subsystem with power network, DC subsystem with power network, and hydrogen subsystem with one hydrogen bus. A bidirectional converter (BC) is connected between the AC bus and DC bus. The AC power sources are diesel engines (DEs) and wind turbines (WTs). The WT, characterized by variable frequency, requires a converter (included in the WT) to connect to AC bus. The DE is the only backup power source in the AC subsystem of the isolated electricity-hydrogen MG. Photovoltaic (PV) arrays and hydrogen fuel cells (HFCs) play roles in the DC power supply.

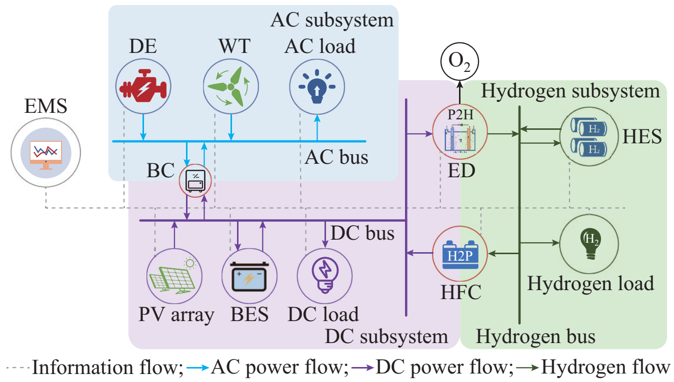

Fig. 1. System architecture of isolated electricity-hydrogen MG.

Similarly, the hydrogen bus is the backbone for hydrogen flow. An electrolyzer device (ED) produces hydrogen, which can consume surplus electricity generated by the WT and PV. In addition, BES in the DC subsystem and HES in the hydrogen subsystem collectively form the hybrid ESS in the isolated electricity-hydrogen MG. They coordinate with each other to deal with the daily power and inter-day energy imbalance of MG. EMS is the control center, which manages each module of the isolated electricity-hydrogen MG. High-voltage hydrogen storage tanks and lithium-ion batteries are currently the most mature and widely used storage devices for hydrogen energy and battery energy, respectively.

The production-consumption balance and power flow constraints of the isolated electricity-hydrogen MG are represented in (1)-(14). Specifically, constraints (1)-(8) are the power balance and power flow constraints of AC subsystems [29]. Constraints (9)-(14) are the power balance and power flow constraints of DC subsystems. The DC power flow constraints are similar to the AC power flow constraints, and we obtain the DC network operation constraints by excluding equations or terms related to reactive power [30]. Equation (15) guarantees the hydrogen flow balance of hydrogen subsystem without power network. It should be noted that, unless otherwise specified, the value of t is assumed to be an integer from 1 to T.

$$P_{\text{AC}}^{t,j}=P_{\text{WT}}^{t,j}+P_{\text{DE}}^{t,j}+(P_{\text{B2A}}^{t,j}-P_{\text{A2B}}^{t,j})-P_{\text{AL}}^{t,j}\quad \forall t,\forall j\in N \tag{1}$$

$$Q_{\text{AC}}^{t,j}=Q_{\text{WT}}^{t,j}+Q_{\text{DE}}^{t,j}+Q_{\text{BC}}^{t,j}-Q_{\text{AL}}^{t,j}\quad \forall t,\forall j\in N \tag{2}$$

$$P_{\text{AC}}^{t,j}=\sum_{k:j\rightarrow k}P_{jk}^{t}-\sum_{i:i\rightarrow j}(P_{ij}^{t}-r_{ij}l_{ij}^{t})\quad \forall t,\forall j\in N \tag{3}$$

$$Q_{\text{AC}}^{t,j}=\sum_{k:j\rightarrow k}Q_{jk}^{t}-\sum_{i:i\rightarrow j}(Q_{ij}^{t}-x_{ij}l_{ij}^{t})\quad \forall t,\forall j\in N \tag{4}$$

$$v^{t,j}=v^{t,i}-2(r_{ij}P_{ij}^{t}+x_{ij}Q_{ij}^{t})+(r_{ij}^{2}+x_{ij}^{2})l_{ij}^{t}\quad \forall t,\ \forall(i,j)\in\varepsilon_N \tag{5}$$

$$\left\|\begin{matrix}2P_{ij}^{t}\\ 2Q_{ij}^{t}\\ l_{ij}^{t}-v^{t,i}\end{matrix}\right\|_2\leq l_{ij}^{t}+v^{t,i}\quad \forall t,\forall(i,j)\in\varepsilon_N \tag{6}$$

$$v_{\min}\leq v^{t,j}\leq v_{\max}\quad \forall t,\forall j\in N \tag{7}$$

$$(P_{ij}^{t})^{2}+(Q_{ij}^{t})^{2}\leq S_{ij,\text{AC},\max}^{2}\quad \forall t,\forall(i,j)\in\varepsilon_N \tag{8}$$

$$\begin{aligned}P_{\text{DC}}^{t,j}=P_{\text{PV}}^{t,j}+(P_{\text{HFC}}^{t,j}-P_{\text{ED}}^{t,j})+(P_{\text{B,dch}}^{t,j}-P_{\text{B,ch}}^{t,j})+\\(P_{\text{B2D}}^{t,j}-P_{\text{D2B}}^{t,j})-P_{\text{DL}}^{t,j}\quad \forall t,\forall j\in M\end{aligned} \tag{9}$$

$$P_{\text{DC}}^{t,j}=\sum_{k:j\rightarrow k}P_{jk}^{t}-\sum_{i:i\rightarrow j}(P_{ij}^{t}-r_{ij}l_{ij}^{t})\quad \forall t,\forall j\in M \tag{10}$$

$$v^{t,j}=v^{t,i}-2r_{ij}P_{ij}^{t}+r_{ij}^{2}l_{ij}^{t}\quad \forall t,\forall(i,j)\in\varepsilon_M \tag{11}$$

$$\left\|\begin{matrix}2P_{ij}^{t}\\ l_{ij}^{t}-v^{t,i}\end{matrix}\right\|_2\leq l_{ij}^{t}+v^{t,i}\quad \forall t,\forall(i,j)\in\varepsilon_M \tag{12}$$

$$v_{\min}\leq v^{t,j}\leq v_{\max}\quad \forall t,\forall j\in M \tag{13}$$

$$(P_{ij}^{t})^{2}\leq P_{ij,\text{DC},\max}^{2}\quad \forall t,\forall(i,j)\in\varepsilon_M \tag{14}$$

$$G_{\text{ED}}^{t}+G_{\text{H,dch}}^{t}=G_{\text{HL}}^{t}+G_{\text{HFC}}^{t}+G_{\text{H,ch}}^{t}\quad \forall t \tag{15}$$

B. Modeling of Coupling Devices

In the isolated electricity-hydrogen MG, the coupling devices composed of BC, ED, and HFC are responsible for the energy conversion between different energy subsystems.

1) BC

The BC undertakes the bidirectional power conversion between AC and DC subsystems. Equations (16) and (17) define the conversion efficiencies of DC to AC (D2A) and AC to DC (A2D) via BC, respectively. The operation of BC needs to meet power capacity constraints in (18) and (19) and power fluctuation constraint (20) [24]. According to [31], the active-reactive relation of BC is defined by constraint (21), and its reactive power Q_{BC}^{t} is limited not only by the active power but also by its capacity S_{BC}.

$$P_{\text{B2A}}^{t}=\eta_{\text{BC,D2A}}P_{\text{D2B}}^{t}\quad \forall t \tag{16}$$

$$P_{\text{B2D}}^{t}=\eta_{\text{BC,A2D}}P_{\text{A2B}}^{t}\quad \forall t \tag{17}$$

$$0\leq P_{\text{D2B}}^{t}\leq P_{\text{D2B,max}}u_{\text{BC}}^{t}\quad \forall t \tag{18}$$

$$0\leq P_{\text{A2B}}^{t}\leq P_{\text{A2B,max}}(1-u_{\text{BC}}^{t})\quad \forall t \tag{19}$$

$$-\Delta P_{\text{BC,dw}}^{\Delta t}\leq(P_{\text{A2B}}^{t}-P_{\text{A2B}}^{t-1})-(P_{\text{D2B}}^{t}-P_{\text{D2B}}^{t-1})\leq\Delta P_{\text{BC,up}}^{\Delta t}\quad \forall t \tag{20}$$

$$(Q_{\text{BC}}^{t})^{2}+(P_{\text{B2A}}^{t}-P_{\text{A2B}}^{t})^{2}\leq S_{\text{BC}}^{2}\quad \forall t \tag{21}$$

2) ED

The ED is responsible for P2H. EDs have good fluctuation adaptability [32]. Among various electrolysis techniques, the alkaline electrolysis (AE) technique is mature and has broad applications [21]. The conversion function of the electrolytic process is shown in (22) [20]. The electrolytic process is powered by electricity, which produces hydrogen and oxygen. Constraint (23) displays the maximum and minimum operating power limits. ED also needs to consider the power ramp rates, as shown in (24).

$$G_{\text{ED}}^{t}=\frac{3.6P_{\text{ED}}^{t}\eta_{\text{ED}}}{V_{\text{HHV}}}\quad \forall t \tag{22}$$

$$P_{\text{ED,min}}u_{\text{ED}}^{t}\leq P_{\text{ED}}^{t}\leq P_{\text{ED,max}}u_{\text{ED}}^{t}\quad \forall t \tag{23}$$

$$-\Delta P_{\text{ED,dw}}^{\Delta t}\leq P_{\text{ED}}^{t}-P_{\text{ED}}^{t-1}-P_{\text{ED,min}}(u_{\text{ED}}^{t}-u_{\text{ED}}^{t-1})\leq\Delta P_{\text{ED,up}}^{\Delta t}\quad \forall t \tag{24}$$

3) HFC

As the facility of hydrogen to power (H2P), the HFC can participate in the reliable operation of MG as a flexible power source [33]. The HFC is modeled similarly to DE. Equation (25) defines that the HFC produces electricity by consuming hydrogen. Constraints (26) and (27) represent the operating power limit and power ramp limit of HFC, respectively.

$$P_{\mathrm{HFC}}^{t}=\frac{G_{\mathrm{HFC}}^{t}V_{\mathrm{HHV}}\eta_{\mathrm{HFC}}}{3.6}\quad \forall t \tag{25}$$

$$P_{\mathrm{HFC,min}}u_{\mathrm{HFC}}^{t}\leq P_{\mathrm{HFC}}^{t}\leq P_{\mathrm{HFC,max}}u_{\mathrm{HFC}}^{t}\quad \forall t \tag{26}$$

$$-\Delta P_{\mathrm{HFC,dw}}^{\Delta t}\leq P_{\mathrm{HFC}}^{t}-P_{\mathrm{HFC}}^{t-1}-P_{\mathrm{HFC,min}}(u_{\mathrm{HFC}}^{t}-u_{\mathrm{HFC}}^{t-1})\leq \Delta P_{\mathrm{HFC,up}}^{\Delta t}\quad \forall t \tag{27}$$

C. Modeling of Energy Storage

The hybrid battery-hydrogen ESS plays a vital role in the isolated electricity-hydrogen MG with high penetration of RESs. The HES is used as a long-term energy storage to realize the inter-day energy balance of the MG, while the BES is used as a short-term energy storage to realize the daily power balance. They correspond to the annual and daily horizons of optimal scheduling, respectively.

1) HES

Although the conversion efficiency between electrical energy and hydrogen energy is not high, hydrogen can be stored on a large scale with high efficiency [34]. The daily self-loss rate of the HES is assumed to be negligible. Equation (28) represents the hydrogen storage process, where the hydrogen is compressed and stored in some periods and released in other periods [20]. Constraints (29) and (30) impose the maximum flow limits on the hydrogen charging and discharging, respectively. By using binary variable u_{H}^{t}, simultaneous charging and discharging are avoided. Constraint (31) describes that the state-of-hydrogen (SOH) must fall within the set range. The MG deploys high-pressure gaseous type II hydrogen storage tanks. The compressor is installed near the filling port of the hydrogen storage tank, and its compression efficiency is included in the charging/discharging efficiency of HES.

$$S_{\mathrm{H}}^{t}=S_{\mathrm{H}}^{t-1}+\Delta t\frac{G_{\mathrm{H,ch}}^{t}\eta_{\mathrm{H,ch}}-\dfrac{G_{\mathrm{H,dch}}^{t}}{\eta_{\mathrm{H,dch}}}}{C_{\mathrm{ap,H}}}\quad \forall t \tag{28}$$

$$0\leq G_{\mathrm{H,ch}}^{t}\leq G_{\mathrm{H,ch,max}}u_{\mathrm{H}}^{t}\quad \forall t \tag{29}$$

$$0\leq G_{\mathrm{H,dch}}^{t}\leq G_{\mathrm{H,dch,max}}(1-u_{\mathrm{H}}^{t})\quad \forall t \tag{30}$$

$$S_{\mathrm{H,min}}\leq S_{\mathrm{H}}^{t}\leq S_{\mathrm{H,max}}\quad \forall t \tag{31}$$

2) BES

Equation (32) describes the dynamic state-of-charge (SOC) balance of the BES [28]. The self-discharging rate of BES is considered. In each time interval, the charging power and discharging power of BES are restricted by the maximum power limits in constraints (33) and (34), respectively. The charging and discharging states of BES are mutually exclusive, by using a binary variable u_{B}^{t}. Constraint (35) represents the specified range of SOCs. Constraint (36) guarantees the initial SOC of the cyclical operation of BES for the next day.

$$S_{\mathrm{B}}^{t}=S_{\mathrm{B}}^{t-1}(1-\eta_{\mathrm{B,self}}\Delta t)+\Delta t\frac{P_{\mathrm{B,ch}}^{t}\eta_{\mathrm{B,ch}}-\dfrac{P_{\mathrm{B,dch}}^{t}}{\eta_{\mathrm{B,dch}}}}{C_{\mathrm{ap,B}}}\quad \forall t \tag{32}$$

$$0\leq P_{\mathrm{B,ch}}^{t}\leq P_{\mathrm{B,ch,max}}u_{\mathrm{B}}^{t}\quad \forall t \tag{33}$$

$$0\leq P_{\mathrm{B,dch}}^{t}\leq P_{\mathrm{B,dch,max}}(1-u_{\mathrm{B}}^{t})\quad \forall t \tag{34}$$

$$S_{\mathrm{B,min}}\leq S_{\mathrm{B}}^{t}\leq S_{\mathrm{B,max}}\quad \forall t \tag{35}$$

$$S_{\mathrm{B}}^{T}\geq S_{\mathrm{B}}^{\mathrm{ini}} \tag{36}$$

D. Modeling of Power Generation

In the isolated electricity-hydrogen MG, power sources consist of RESs and DEs. Wind-solar RESs are the zero-carbon power generation equipment in the MG. However, due to the intermittent nature of the output of RES, it is necessary to deploy DEs to meet the reliability requirement of the power supply in the MG.

1) DE

The DE is the only controllable backup power source of the MG. The participation of DEs in the dispatch requires a trade-off between economy and reliability due to their expensive fuel cost and carbon emissions. Constraints (37) and (38) limit the operating power range and power adjustment, respectively [24]. The maximum and minimum continuous operating durations are limited in (39) and (40), respectively, and the minimum continuous shutdown duration is limited by (41) [28]. Constraint (42) defines that the active power and reactive power of the DE are limited by its capacity [31]. The fuel consumption is formulated as a linear function (43) [35].

$$P_{\mathrm{DE,min}}u_{\mathrm{DE}}^{t}\leq P_{\mathrm{DE}}^{t}\leq P_{\mathrm{DE,max}}u_{\mathrm{DE}}^{t}\quad \forall t \tag{37}$$

$$-\Delta P_{\mathrm{DE,dw}}^{\Delta t}\leq P_{\mathrm{DE}}^{t}-P_{\mathrm{DE}}^{t-1}-P_{\mathrm{DE,min}}(u_{\mathrm{DE}}^{t}-u_{\mathrm{DE}}^{t-1})\leq \Delta P_{\mathrm{DE,up}}^{\Delta t}\quad \forall t \tag{38}$$

$$\sum_{i=-D_{\max}^{\mathrm{on},\Delta t}}^{0}u_{\mathrm{DE}}^{t+i}\leq D_{\max}^{\mathrm{on},\Delta t}\quad \forall t\in[1,2,...,2T] \tag{39}$$

$$\sum_{i=1-D_{\min}^{\mathrm{on},\Delta t}}^{0}u_{\mathrm{DE}}^{t+i}\geq D_{\min}^{\mathrm{on},\Delta t}(u_{\mathrm{DE}}^{t-D_{\min}^{\mathrm{on},\Delta t}+1}-u_{\mathrm{DE}}^{t-D_{\min}^{\mathrm{on},\Delta t}})\quad \forall t\in[1,2,...,2T] \tag{40}$$

$$\sum_{i=1-D_{\min}^{\mathrm{off},\Delta t}}^{0}(1-u_{\mathrm{DE}}^{t+i})\geq D_{\min}^{\mathrm{off},\Delta t}(u_{\mathrm{DE}}^{t-D_{\min}^{\mathrm{off},\Delta t}}-u_{\mathrm{DE}}^{t-D_{\min}^{\mathrm{off},\Delta t}+1})\quad \forall t\in[1,2,...,2T] \tag{41}$$

$$(Q_{\mathrm{DE}}^{t})^{2}+(P_{\mathrm{DE}}^{t})^{2}\leq S_{\mathrm{DE}}^{2}u_{\mathrm{DE}}^{t}\quad \forall t \tag{42}$$

$$F_{\mathrm{fuel}}^{t}=F_{1}P_{\mathrm{DE,r}}u_{\mathrm{DE}}^{t}+F_{2}P_{\mathrm{DE}}^{t} \tag{43}$$

2) RES

Most previous works indicate that the power output of PV mainly depends on the ambient temperature and solar radiation intensity [36], and that of WT can be estimated from the wind speed [37]. Since these influencing factors are uncontrollable, the power output of RES is uncertain. This paper only focuses on the predicted outputs of RESs participating in MG dispatch on different time scales. As shown in (44), the dispatch power of RESs are all less than or equal to the maximum outputs of the RESs, which may result in excess generation curtailment. The WT located in the AC subsystem can provide reactive power with an output range given by constraint (45) [31].

$$\begin{cases}0\leq P_{\mathrm{PV}}^{t}\leq P_{\mathrm{PVG}}^{t}\quad \forall t\\ 0\leq P_{\mathrm{WT}}^{t}\leq P_{\mathrm{WTG}}^{t}\quad \forall t\end{cases} \tag{44}$$

$$(Q_{\mathrm{WT}}^{t})^{2}+(P_{\mathrm{WT}}^{t})^{2}\leq S_{\mathrm{WT}}^{2}\quad \forall t \tag{45}$$

E. Modeling of Load Demand

The load demand of the isolated electricity-hydrogen MG consists of AC loads, DC loads, and hydrogen loads. In order to ensure the stable operation of the isolated electricity-hydrogen MG, each type of load can be divided into critical and cuttable loads. In addition, a demand response program is considered for curtailing loads. The operator needs to pay extra costs for the load curtailment participation [25], [38]. Constraint (46) represents the range of load supply. Equation (47) defines the load curtailment of each type of load. The expression of AC load is given by (48).

$$\begin{cases} P^t_{\mathrm{DL,A}} \leq P^t_{\mathrm{DL}} \leq P^t_{\mathrm{DL,A\&B}} & \forall t \\ P^t_{\mathrm{AL,A}} \leq P^t_{\mathrm{AL}} \leq P^t_{\mathrm{AL,A\&B}} & \forall t \\ G^t_{\mathrm{HL,A}} \leq G^t_{\mathrm{HL}} \leq G^t_{\mathrm{HL,A\&B}} & \forall t \end{cases} \tag{46}$$

$$\begin{cases} P^t_{\mathrm{DL,cur}} = P^t_{\mathrm{DL,A\&B}} - P^t_{\mathrm{DL}} & \forall t \\ P^t_{\mathrm{AL,cur}} = P^t_{\mathrm{AL,A\&B}} - P^t_{\mathrm{AL}} & \forall t \\ G^t_{\mathrm{HL,cur}} = G^t_{\mathrm{HL,A\&B}} - G^t_{\mathrm{HL}} & \forall t \end{cases} \tag{47}$$

$$Q^t_{\mathrm{AL}} = P^t_{\mathrm{AL}} \tan(\arccos \gamma_{\mathrm{AL}}) \quad \forall t \tag{48}$$

III. Dispatch Problem Formulation

A. Proposed Method

The proposed method has a similar framework to the multi-time-scale rolling scheduling strategy. The proposed method consists of two dispatch horizons: the annual horizon (inter-day energy dispatch) and the daily horizon (day-ahead power dispatch). The flowchart of the proposed method is shown in Fig. 2.

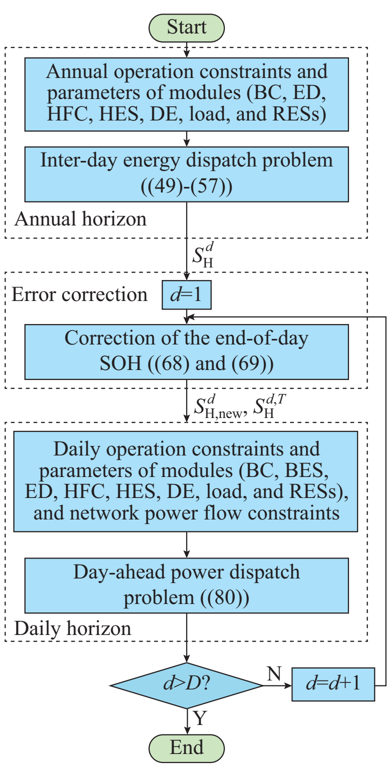

Fig. 2. Flowchart of proposed method.

The proposed method first carries out the inter-day energy dispatch, and then iteratively conducts the day-ahead power dispatch throughout the year.

The proposed method has two main improvements: ① we conduct a full-year low-carbon dispatch for an isolated electricity-hydrogen MG with high penetration of RESs; ② the inter-day energy dispatch belongs to forward-looking dispatch, which aims to obtain the annual distribution of hydrogen storage state constraints and exchange them as boundary information with the lower-level dispatch.

Prior to carrying out the day-ahead power dispatch problem, it is necessary to obtain the latest end-of-day SOH. We calculate the errors between the estimated annual energy production and consumption data and the day-ahead forecast data. It aims to correct the end-of-day SOH constraint for the day-ahead power dispatch through the hydrogen energy transmission chain.

B. Annual Horizon: Inter-day Energy Dispatch

For an isolated electricity-hydrogen MG with high penetration of RESs, there are significant differences in its energy production and consumption characteristics across different seasons, and there are also differences between weekdays and weekends/holidays. Existing short-term dispatch methods such as day-ahead dispatching cannot effectively deal with the seasonal and daily energy differences in such an isolated electricity-hydrogen MG. To address these mismatches, this paper uses HES as seasonal energy storage and achieves long-term cross-seasonal and cross-day energy balance of isolated electricity-hydrogen MGs through inter-day energy dispatch.

The annual horizon is used for the inter-day energy dispatch based on the estimated year-ahead energy data. The problem of seasonal energy mismatch is solved by obtaining the boundary conditions of HES. A high resolution (high level of details and granularity) in the annual horizon would produce a large number of optimization variables. Moreover, the accurate forecast of high-resolution data for the following year is not available. Therefore, the annual horizon model is an inter-day energy dispatch model.

The power and hydrogen flows of the inter-day energy dispatch are shown in Fig. 3. Each day is a time node in the annual horizon model. A daily energy data set of RESs and loads is considered to capture the end-of-day SOH of HES throughout the year. The dispatch model of annual horizon needs to consider the daily energy constraints and daily operational costs of each module instead of the intraday operational details. In addition, the batteries are not considered in the model since they perform only intraday cycles.

The objective of the dispatch model in the annual horizon is to minimize the annual operational cost C_{year}, which relates to BC, ED, HFC, RESs, DE, HES, and load curtailment, as shown in (49). Equation (50) represents the energy balance constraints of AC, DC, and hydrogen subsystems. The daily energy constraints of BC, ED, HFC, HES, DE, RESs, and load curtailment are represented in (51)-(57), respectively.

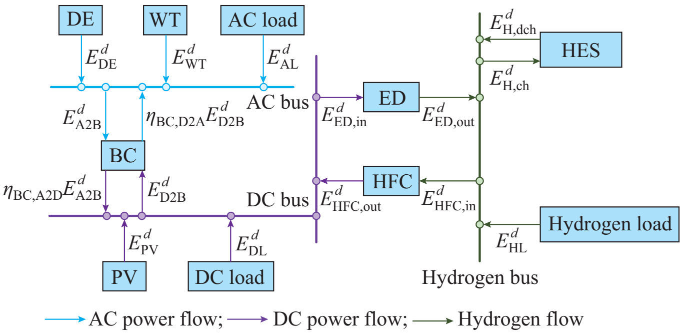

Fig. 3. Power and hydrogen flows of inter-day energy dispatch.

$$\begin{aligned}\min C_{\text{year}}=&\sum_{d=1}^{D} m_{\text{BC}}^{\text{O\&M}}(E_{\text{A2B}}^{d}+E_{\text{D2B}}^{d})+\sum_{d=1}^{D}(m_{\text{ED}}^{\text{O\&M}}+m_{\text{ED}}^{\text{dep}})E_{\text{ED,in}}^{d}+\\&\sum_{d=1}^{D}(m_{\text{HFC}}^{\text{O\&M}}+m_{\text{HFC}}^{\text{dep}})E_{\text{HFC,out}}^{d}+\sum_{d=1}^{D}C_{\text{DE}}^{d}(u_{\text{DE}}^{t},E_{\text{DE}}^{d})+\\&\sum_{d=1}^{D}(m_{\text{PV}}^{\text{O\&M}}E_{\text{PV}}^{d}+m_{\text{WT}}^{\text{O\&M}}E_{\text{WT}}^{d})+\\&\sum_{d=1}^{D}(m_{\text{H}}^{\text{O\&M}}+m_{\text{H}}^{\text{dep}})(E_{\text{H,ch}}^{d}+E_{\text{H,dch}}^{d})+\\&\sum_{d=1}^{D}[m_{\text{EL}}^{\text{cur}}(E_{\text{DL,A\&B}}^{d}+E_{\text{AL,A\&B}}^{d}-E_{\text{DL}}^{d}-E_{\text{AL}}^{d})+\\&m_{\text{HL}}^{\text{cur}}(E_{\text{HL,A\&B}}^{d}-E_{\text{HL}}^{d})]\end{aligned}\tag{49}$$

s.t.

$$\begin{cases}E_{\text{WT}}^{d}+E_{\text{DE}}^{d}+\eta_{\text{BC,D2A}}E_{\text{D2B}}^{d}=E_{\text{AL}}^{d}+E_{\text{A2B}}^{d} & \forall d\\E_{\text{PV}}^{d}+E_{\text{HFC,out}}^{d}+\eta_{\text{BC,A2D}}E_{\text{A2B}}^{d}=E_{\text{DL}}^{d}+E_{\text{ED,in}}^{d}+E_{\text{D2B}}^{d} & \forall d\\E_{\text{ED,out}}^{d}+E_{\text{H,dch}}^{d}=E_{\text{HL}}^{d}+E_{\text{HFC,in}}^{d}+E_{\text{H,ch}}^{d} & \forall d\end{cases}\tag{50}$$

$$\begin{cases}0\le E_{\text{D2B}}^{d}\le \Delta tTP_{\text{D2B,max}}u_{\text{BC}}^{d} & \forall d\\0\le E_{\text{A2B}}^{d}\le \Delta tTP_{\text{A2B,max}}(1-u_{\text{BC}}^{d}) & \forall d\end{cases}\tag{51}$$

$$\begin{cases}\Delta tP_{\text{ED,min}}u_{\text{ED}}^{d}\le E_{\text{ED,in}}^{d}\le \Delta tTP_{\text{ED,max}}u_{\text{ED}}^{d} & \forall d\\E_{\text{ED,out}}^{d}=\dfrac{3.6E_{\text{ED,in}}^{d}\eta_{\text{ED}}}{V_{\text{HHV}}} & \forall d\end{cases}\tag{52}$$

$$\begin{cases}\Delta tP_{\text{HFC,min}}u_{\text{HFC}}^{d}\le E_{\text{HFC,out}}^{d}\le \Delta tTP_{\text{HFC,max}}u_{\text{HFC}}^{d} & \forall d\\E_{\text{HFC,in}}^{d}=\dfrac{3.6E_{\text{HFC,out}}^{d}}{V_{\text{HHV}}\eta_{\text{HFC}}} & \forall d\end{cases}\tag{53}$$

$$\begin{cases}0\le E_{\text{H,ch}}^{d}\le \Delta tTG_{\text{H,ch,max}}u_{\text{H}}^{d} & \forall d\\0\le E_{\text{H,dch}}^{d}\le \Delta tTG_{\text{H,dch,max}}(1-u_{\text{H}}^{d}) & \forall d\\S_{\text{H}}^{d}=S_{\text{H}}^{d-1}(1-\eta_{\text{H,self}})+\dfrac{E_{\text{H,ch}}^{d}\eta_{\text{H,ch}}-\dfrac{E_{\text{H,dch}}^{d}}{\eta_{\text{H,dch}}}}{C_{\text{ap,H}}} & \forall d\\S_{\text{H,min}}\le S_{\text{H}}^{d}\le S_{\text{H,max}} & \forall d\\S_{\text{H}}^{D}\ge S_{\text{H}}^{\text{ini}}\end{cases}\tag{54}$$

$$E_{\text{DE,min}}u_{\text{DE}}^{d}\le E_{\text{DE}}^{d}\le E_{\text{DE,max}}u_{\text{DE}}^{d}\quad \forall d\tag{55}$$

$$\begin{cases}0\le E_{\text{PV}}^{d}\le E_{\text{PVG}}^{d} & \forall d\\0\le E_{\text{WT}}^{d}\le E_{\text{WTG}}^{d} & \forall d\end{cases}\tag{56}$$

$$\begin{cases}E_{\text{DL,A}}^{d}\le E_{\text{DL}}^{d}\le E_{\text{DL,A\&B}}^{d} & \forall d\\E_{\text{AL,A}}^{d}\le E_{\text{AL}}^{d}\le E_{\text{AL,A\&B}}^{d} & \forall d\\E_{\text{HL,A}}^{d}\le E_{\text{HL}}^{d}\le E_{\text{HL,A\&B}}^{d} & \forall d\end{cases}\tag{57}$$

The daily operational cost of DE C_{DE}^{d} in (49) is directly related to daily generation, operating time, and start-up time, as shown in (58). Since the dispatch model of annual horizon does not consider power details, the daily operational cost function of DE is simplified in (59).

$$\begin{aligned}C_{\text{DE}}^{d}(u_{\text{DE}}^{t},E_{\text{DE}}^{d})=&(m_{\text{DE}}^{\text{O\&M}}+\pi_{C}c_{\text{G}}F_{2}+V_{\text{DE}}^{\text{fuel}}F_{2})E_{\text{DE}}^{d}+\\&(V_{\text{DE}}^{\text{fuel}}+\pi_{C}c_{\text{G}})F_{1}P_{\text{DE,r}}\Delta t\sum_{t=1}^{T}u_{\text{DE}}^{t}+V_{\text{DE}}^{\text{start}}\sum_{t=1}^{T}u_{\text{DE}}^{t}(1-u_{\text{DE}}^{t-1})\end{aligned}\tag{58}$$

$$C_{\text{DE}}^{d}(u_{\text{DE}}^{t},E_{\text{DE}}^{d})\approx a_{\text{DE}}E_{\text{DE}}^{d}+b_{\text{DE}}u_{\text{DE}}^{d}\tag{59}$$

C. Daily Horizon: Day-ahead Power Dispatch

The daily horizon focuses on the day-ahead power dispatch. Obviously, due to the uncertainty of RESs and load, there are errors between the estimated annual energy production and consumption data and the day-ahead forecast data. The utilization ratio of HES capacity that participates in the dispatch during a single day is very low. Therefore, the daily day-ahead power dispatch can make full use of the idle capacity of HES to deal with the above errors. Equation (60) shows the errors between the estimated annual energy production and consumption data and the day-ahead forecast data of WT, PV, and various loads.

$$\begin{cases}error_{\text{WT}}^{d}=\Delta t\sum_{t=1}^{T}P_{\text{WTG}}^{t}-E_{\text{WT}}^{d}\\error_{\text{PV}}^{d}=\Delta t\sum_{t=1}^{T}P_{\text{PVG}}^{t}-E_{\text{PV}}^{d}\\error_{\text{AL}}^{d}=\Delta t\sum_{t=1}^{T}P_{\text{AL,A\&B}}^{t}-E_{\text{AL}}^{d}\\error_{\text{DL}}^{d}=\Delta t\sum_{t=1}^{T}P_{\text{DL,A\&B}}^{t}-E_{\text{DL}}^{d}\\error_{\text{HL}}^{d}=\Delta t\sum_{t=1}^{T}G_{\text{HL}}^{t}-E_{\text{HL}}^{d}\end{cases}\tag{60}$$

The end-of-day SOH that considers the forecast errors is calculated through the hydrogen energy transmission chain. The specific steps for the influence of forecast errors on the transmission chain of HES energy are represented by (61)-(66). Equation (67) shows the value of SOH variation caused by estimation errors. The end-of-day SOH is calculated by combining the initial SOH, year-ahead SOH plan, SOH variation, and SOH range limit, as shown in (68)-(70).

$$\Delta E_{\text{AC,NG}}^{d}=error_{\text{WT}}^{d}-error_{\text{AL}}^{d}\tag{61}$$

$$\Delta E_{\text{BC,A2B}}^{d}=\begin{cases}\Delta E_{\text{AC,NG}}^{d} & \Delta E_{\text{AC,NG}}^{d}\ge 0\\0 & \Delta E_{\text{AC,NG}}^{d}<0\end{cases}\tag{62a}$$

$$\Delta E_{\text{BC,B2A}}^{d}=\begin{cases}0 & \Delta E_{\text{AC,NG}}^{d}\ge 0\\-\Delta E_{\text{AC,NG}}^{d} & \Delta E_{\text{AC,NG}}^{d}<0\end{cases}\tag{62b}$$

$$\Delta E_{\mathrm{DC,NG}}^{d}=error_{\mathrm{PV}}^{d}-error_{\mathrm{DL}}^{d}+\eta_{\mathrm{BC,A2D}}\Delta E_{\mathrm{BC,A2B}}^{d}-\frac{\Delta E_{\mathrm{BC,B2A}}^{d}}{\eta_{\mathrm{BC,D2A}}} \tag{63}$$

$$\Delta E_{\mathrm{ED}}^{d}=\begin{cases}\Delta E_{\mathrm{DC,NG}}^{d} & \Delta E_{\mathrm{DC,NG}}^{d}\geq 0\\ 0 & \Delta E_{\mathrm{DC,NG}}^{d}<0\end{cases} \tag{64a}$$

$$\Delta E_{\mathrm{HFC}}^{d}=\begin{cases}0 & \Delta E_{\mathrm{DC,NG}}^{d}\geq 0\\ -\Delta E_{\mathrm{DC,NG}}^{d} & \Delta E_{\mathrm{DC,NG}}^{d}<0\end{cases} \tag{64b}$$

$$\Delta E_{\mathrm{H,NG}}^{d}=\frac{3.6\eta_{\mathrm{ED}}\Delta E_{\mathrm{ED}}^{d}}{V_{\mathrm{HHV}}}-\frac{3.6\Delta E_{\mathrm{HFC}}^{d}}{V_{\mathrm{HHV}}\eta_{\mathrm{HFC}}}-error_{\mathrm{HL}}^{d} \tag{65}$$

$$\Delta E_{\mathrm{H,ch}}^{d}=\begin{cases}\Delta E_{\mathrm{H,NG}}^{d} & \Delta E_{\mathrm{H,NG}}^{d}\geq 0\\ 0 & \Delta E_{\mathrm{H,NG}}^{d}<0\end{cases} \tag{66a}$$

$$\Delta E_{\mathrm{H,dch}}^{d}=\begin{cases}0 & \Delta E_{\mathrm{H,NG}}^{d}\geq 0\\ -\Delta E_{\mathrm{H,NG}}^{d} & \Delta E_{\mathrm{H,NG}}^{d}<0\end{cases} \tag{66b}$$

$$\Delta S_{\mathrm{H,error}}^{d}=\frac{\Delta E_{\mathrm{H,ch}}^{d}\eta_{\mathrm{H,ch}}-\dfrac{\Delta E_{\mathrm{H,dch}}^{d}}{\eta_{\mathrm{H,dch}}}}{C_{\mathrm{ap,H}}} \tag{67}$$

$$\zeta_{\mathrm{H}}^{d}=S_{\mathrm{H}}^{d,0}+(S_{\mathrm{H}}^{d}-S_{\mathrm{H}}^{d-1})+\Delta S_{\mathrm{H,error}}^{d} \tag{68}$$

$$S_{\mathrm{H,new}}^{d}=\begin{cases}\zeta_{\mathrm{H}}^{d} & S_{\mathrm{H}}^{d}-\zeta_{\mathrm{H}}^{d}\leq\varepsilon_{\mathrm{SOH,max}}\\ S_{\mathrm{H}}^{d}-\varepsilon_{\mathrm{SOH,max}} & S_{\mathrm{H}}^{d}-\zeta_{\mathrm{H}}^{d}>\varepsilon_{\mathrm{SOH,max}}\end{cases} \tag{69}$$

$$\begin{cases}S_{\mathrm{H}}^{d,T}\geq S_{\mathrm{H,new}}^{d} & S_{\mathrm{H,min}}<S_{\mathrm{H,new}}^{d}<S_{\mathrm{H,max}}\\ S_{\mathrm{H}}^{d,T}\geq S_{\mathrm{H,max}} & S_{\mathrm{H,new}}^{d}\geq S_{\mathrm{H,max}}\\ S_{\mathrm{H}}^{d,T}\geq S_{\mathrm{H,min}} & S_{\mathrm{H,new}}^{d}\leq S_{\mathrm{H,min}}\end{cases} \tag{70}$$

The daily operational cost C_{day} in (71) is proposed. It should be noted that the total operational cost consists of the operational and maintenance costs for each module. In addition, considering that the operation of energy storage directly affects the depreciation cost, we include the depreciation cost of energy storage. Other fixed investment costs are not included in the optimization objective. Equation (72) denotes the operational cost of BC C_{BC}. The operational cost of DE C_{DE} composed of maintenance cost, start-up cost, diesel cost, and environmental cost are defined in (73). Equation (74) defines the operational cost of RESs C_{RESs}. Equation (75) denotes the total payment for curtailing loads C_{Load}. Unlike other devices, the operational cost of BES includes maintenance cost and depreciation cost, in which the energy throughput calculates the depreciation price. Equation (76) denotes the operational cost of BES C_{B}. Equation (77) defines the operational cost of ED C_{ED}. Similarly, the operational cost of HFC C_{HFC} is related to the operating power through (78). Equation (79) defines the operational cost of HES C_{H}.

$$C_{\mathrm{day}}=C_{\mathrm{BC}}+C_{\mathrm{DE}}+C_{\mathrm{RES}}+C_{\mathrm{Load}}+C_{\mathrm{B}}+C_{\mathrm{ED}}+C_{\mathrm{HFC}}+C_{\mathrm{H}} \tag{71}$$

$$C_{\mathrm{BC}}=m_{\mathrm{BC}}^{\mathrm{O\&M}}\sum_{t=1}^{T}\Delta t(P_{\mathrm{A2B}}^{t}+P_{\mathrm{D2B}}^{t}) \tag{72}$$

$$C_{\mathrm{DE}}=m_{\mathrm{DE}}^{\mathrm{O\&M}}\sum_{t=1}^{T}\Delta tP_{\mathrm{DE}}^{t}+V_{\mathrm{DE}}^{\mathrm{start}}\sum_{t=1}^{T}u_{\mathrm{DE}}^{t}(1-u_{\mathrm{DE}}^{t-1})+V_{\mathrm{DE}}^{\mathrm{fuel}}\sum_{t=1}^{T}\Delta tF_{\mathrm{fuel}}^{t}+\pi_{C}c_{\mathrm{G}}\sum_{t=1}^{T}\Delta tF_{\mathrm{fuel}}^{t} \tag{73}$$

$$C_{\mathrm{RES}}=m_{\mathrm{PV}}^{\mathrm{O\&M}}\sum_{t=1}^{T}\Delta tP_{\mathrm{PV}}^{t}+m_{\mathrm{WT}}^{\mathrm{O\&M}}\sum_{t=1}^{T}\Delta tP_{\mathrm{WT}}^{t} \tag{74}$$

$$C_{\mathrm{Load}}=m_{\mathrm{EL}}^{\mathrm{cur}}\sum_{t=1}^{T}\Delta t(P_{\mathrm{DL,cur}}^{t}+P_{\mathrm{AL,cur}}^{t})+m_{\mathrm{HL}}^{\mathrm{cur}}\sum_{t=1}^{T}\Delta tG_{\mathrm{HL,cur}}^{t} \tag{75}$$

$$C_{\mathrm{B}}=\sum_{t=1}^{T}(m_{\mathrm{B}}^{\mathrm{O\&M}}+m_{\mathrm{B}}^{\mathrm{dep}})\Delta t(P_{\mathrm{B,ch}}^{t}+P_{\mathrm{B,dch}}^{t}) \tag{76}$$

$$C_{\mathrm{ED}}=(m_{\mathrm{ED}}^{\mathrm{O\&M}}+m_{\mathrm{ED}}^{\mathrm{dep}})\sum_{t=1}^{T}\Delta tP_{\mathrm{ED}}^{t} \tag{77}$$

$$C_{\mathrm{HFC}}=(m_{\mathrm{HFC}}^{\mathrm{O\&M}}+m_{\mathrm{HFC}}^{\mathrm{dep}})\sum_{t=1}^{T}\Delta tP_{\mathrm{HFC}}^{t} \tag{78}$$

$$C_{\mathrm{H}}=(m_{\mathrm{H}}^{\mathrm{O\&M}}+m_{\mathrm{H}}^{\mathrm{dep}})\sum_{t=1}^{T}\Delta t(G_{\mathrm{H,ch}}^{t}+G_{\mathrm{H,dch}}^{t}) \tag{79}$$

A day-ahead power dispatch model is formulated to carry out the day-ahead power optimization of each module in the MG, which is given as:

$$\begin{cases}\min C_{\mathrm{day}}\\ \text{s.t. (1)-(48), (70), (72)-(79)}\end{cases} \tag{80}$$

In summary, the inter-day energy dispatch model (49)-(57) is modeled as a mixed-integer linear programming (MILP) problem, which is usually solvable and can be solved using conventional solvers. After convexifying the AC/DC power flow model, the day-ahead power dispatch model shown in (80) becomes a mixed-integer second order cone programming (MISOCP) problem, and the solution to such a problem is feasible in both theory and practice. From the perspective of solving, these two types of problems can be solved by a solver to obtain the optimal solution. From the perspective of optimization, the optimality of the decision-making scheme depends on the accuracy of the input data.

IV. Case Studies

The MATLAB 2021a with solvers of GUROBI 10.0.1 and GAMS Studio 37.1.0 with solvers of LINDO [39] are used to solve the MILP and MISOCP problems. All simulation analyses are performed on a computer with an Intel i7-9700 CPU (3.00 GHz), 16 GB RAM, and Windows.

A. Simulation Setup

For case studies, an isolated electricity-hydrogen MG is considered, the topology of which is shown in Fig. 4. Based on the standard IEEE 33-node power system, an isolated electricity-hydrogen MG consisting of a 9-node DC subsystem, a 9-node AC subsystem, and a hydrogen subsystem is selected for case studies, where A1-A9 are nodes 1-9 in the AC subsystem, D1-D9 are nodes 1-9 in the DC subsystem, and H1 is node 1 in the hydrogen subsystem. The DE is deployed at A1. The WT is deployed at A9. In addition, the BES is deployed at D6. The PV is deployed at D7. The HES is deployed at H1. The BC is deployed between A1 and D1. The ED and HFC are both deployed between D2 and H1.

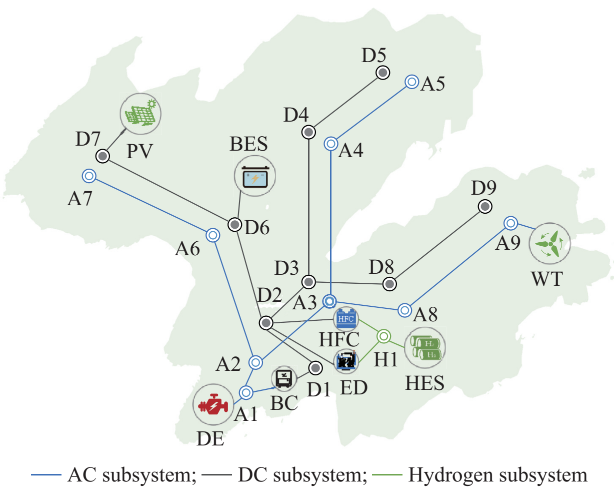

Fig. 4. Topology of isolated electricity-hydrogen MG.

The time resolutions of Δd and Δt are set to be 1 day and 1 hour, respectively. The annual horizon of inter-day energy dispatch is set to be 1 year ($D=365$ days), and the daily horizon of day-ahead power dispatch is set to be 1 day ($T=24$ hours). The original data sets of RES generation and electrical loads are derived from the historical electric data on the online website [40]. The hydrogen demand mainly refers to hydrogen-fueled vehicles, which exhibit similar daily consumption patterns to fossil-fueled vehicles, with minimal variation in demand [41].

To preserve the characteristics of the original data, the source data of 2019 are extracted and scaled. The daily power outputs of WT (200 kW) and PV (1260 kW), daily AC load, and daily hydrogen load are shown in Supplementary Material A Fig. A1. These daily data are considered as the day-ahead forecast data of the isolated electricity-hydrogen MG. In addition, the annual energy curves of RESs and load demand are calculated with a time resolution of one day. The estimated data based on the least squares method are used as the year-ahead forecast data, as shown in Supplementary Material A Fig. A2. Because each type of load is composed of critical and cuttable loads, the maximum cuttable loads are supposed to be one-third of the total loads.

The initial power of BC, ED, HFC, and DE is set to be 0. The initial SOC of BES is set to be 0.3, and the initial SOH of HES is set to be 0.6. The other system parameters of the isolated electricity-hydrogen MG are listed in Supplementary Material A Table AI.

To examine the effect of the proposed method on the decarbonization of isolated electricity-hydrogen MG, three different cases with the same load demand are considered, and their differences are listed in Table I, where high means daily power outputs of WT and PV are 200 kW and 1260 kW, respectively; and super-high means daily power outputs of WT and PV are 200 kW and 1475 kW, respectively.

TABLE I
DIFFERENCES AMONG THREE CASES

Case	RES penetration	BES	HES	HFC	Optimization method
1	High	√	×	×	Day-ahead power dispatch
2	High	√	√	√	Proposed method
3	Super-high	√	√	√	Proposed method

Note: √ and × represent the corresponding device is considered and not considered, respectively.

The daily evaluation indicators for the isolated electricity-hydrogen MG are defined in Supplementary Material A (A1)-(A3), including daily green power ratio $R_{\text{RESs, G}}^{\text{annual}}$, daily RES utilization $R_{\text{RESs, U}}^{\text{annual}}$, and daily demand coverage ratio $R_{\text{Load, S}}^{\text{daily}}$. The seasonal evaluation indicators for the isolated electricity-hydrogen MG are defined in Supplementary Material A (A4)-(A6), including annual green power ratio $R_{\text{RESs, G}}^{\text{annual}}$, annual RES utilization ratio $R_{\text{RESs, U}}^{\text{annual}}$, and annual demand coverage ratio $R_{\text{Load, S}}^{\text{daily}}$. The above evaluation indicators are used to quantitatively compare the performance of three cases.

B. Optimal Results in Case 1

The penetration of RESs in case 1 is high, but the HES and HFC are not considered to be deployed in the isolated electricity-hydrogen MG. The day-ahead power dispatch performance is fully taken into account for the full 365 days of the year. The daily average optimization time is 19.172 s, the annual operating cost is \$368780.55, the annual green power ratio is 68.23%, the annual RES utilization ratio is 73.23%, and the annual demand coverage ratio is 98.41%.

The optimal results of day-ahead power dispatch on January 1 in case 1 can be observed in Fig. 5. As can be observed from Fig. 5(a), the AC subsystem experiences a severe power shortage due to the highly intermittent WT generation. The DE serves as the main power supply source on that day. Meanwhile, the BC needs to transfer part of the electricity generated by the DE to DC subsystem. As shown in Fig. 5(b) and (c), the partial hydrogen load curtailment is found due to RES power shortages and economic considerations. In addition, Fig. 5(b) indicates that the BES can help reduce load curtailment by electricity shifting. Figure 5(c) presents the hydrogen load, which is only supplied by the ED. In this case, the unidirectional hydrogen energy can also be regarded as a kind of electric load. For case 1 on January 1, the total daily operational cost is \$2070.25. The daily green power ratio, daily RES utilization, and daily demand coverage ratio are 20.20%, 100%, and 96.85%, respectively.

The optimal results in case 1 show that integrating a high penetration of RESs into isolated electricity-hydrogen MGs can increase the green power. However, RESs are intermittent power sources. The possibility of energy shortage still exists due to the seasonal nature of their outputs. Therefore, some controllable power generation sources (e. g., DEs) are required to ensure the reliable and economic operation of MG.

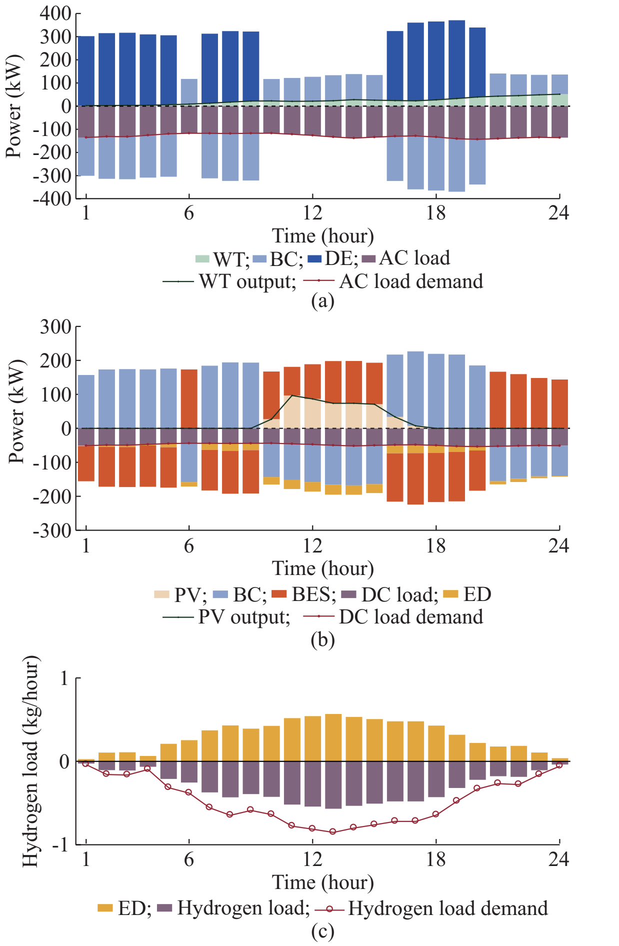

Fig. 5. Optimal results of day-ahead power dispatch on January 1 in case 1. (a) AC subsystem. (b) DC subsystem. (c) Hydrogen subsystem.

C. Optimal Results in Case 2

Unlike case 1, the HES and HFC are considered for deployment in case 2. There is a two-way interaction between hydrogen and electricity. Therefore, the proposed method is also performed in this case.

The optimal results of inter-day energy dispatch in case 2 are displayed in Fig. 6, and the optimization time is 11.868 s. From the perspective of annual horizon, we can see that the energy supply of RESs and load demand also do not always match exactly. As illustrated in Fig. 6(a) and (b), the PV energy is more abundant in the second and third quarters, while electric load demand is relatively low in these two seasons. Figure 6(a) indicates that DEs are needed in this case due to the insufficient penetration of RESs. From day 59 to day 300, some residual PV output is converted into hydrogen and primarily stored in the HES, as shown in Fig. 6(b) and (c). The stored hydrogen energy is released during winter and spring when the electricity supply is limited. The HFC converts the hydrogen energy into electricity to participate in dispatch.

We perform the day-ahead power dispatch for 365 days to obtain the full-year performance. The simulation results show that the daily optimization time ranges from 0.486 s to 553.973 s, with an average optimization time of 17.540 s. In terms of seasonal evaluation indicators for the isolated electricity-hydrogen MG, the annual operating cost is \$276690.24, the annual green power ratio is 84.67%, the annual RES utilization ratio is 99.23%, and the annual demand coverage ratio is 99.34%.

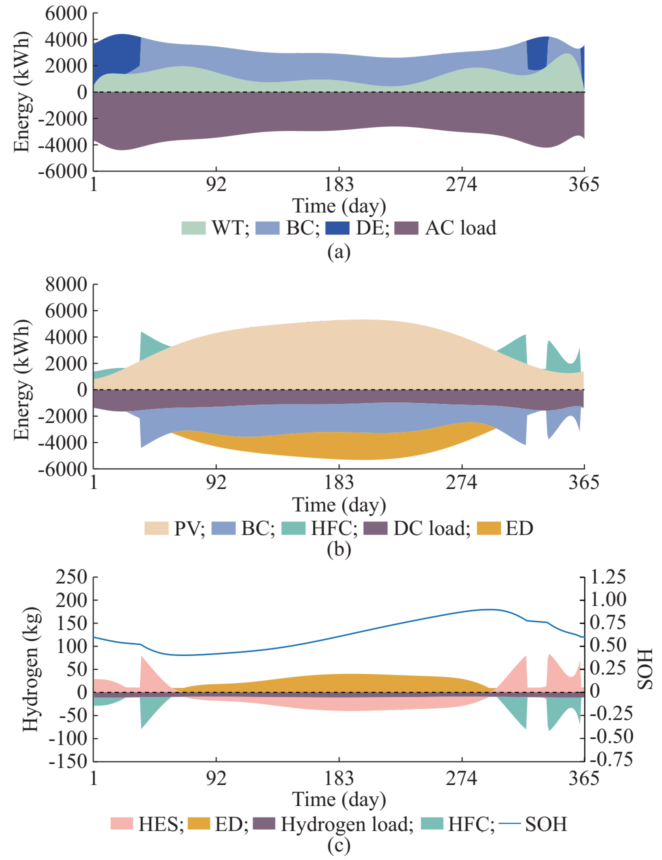

Fig. 6. Optimal results of inter-day energy dispatch in case 2. (a) AC subsystem. (b) DC subsystem. (c) Hydrogen subsystem.

In particular, the day-ahead power dispatch on January 1 is calculated. The optimal results of day-ahead power dispatch in case 2 are shown in Fig. 7. Figure 7(a) shows the day-ahead power dispatch results of the AC subsystem. Compared with case 1, the DE still participates in power dispatch, but its power generation has decreased. This is because the HES releases hydrogen energy, and the HFC provides electricity as a power source, as shown in Fig. 7(b) and (c). The total daily operational cost in case 2 is decreased to \$1667.39. The daily green power ratio, daily RESs utilization, and daily demand coverage ratio are 23.61%, 100%, and 100%, respectively.

From the optimal results of case 2, we can see that the output of RESs also has distinct seasonal characteristics in addition to intraday power fluctuations. Integrating HESs and HFCs makes the isolated electricity-hydrogen MG change from a power system to an electricity-hydrogen coupling system. The interaction with the hydrogen subsystem can alleviate the seasonal mismatch created by integrating a high penetration of RESs. In addition, both dispatch economy and operational reliability are also improved in this case.

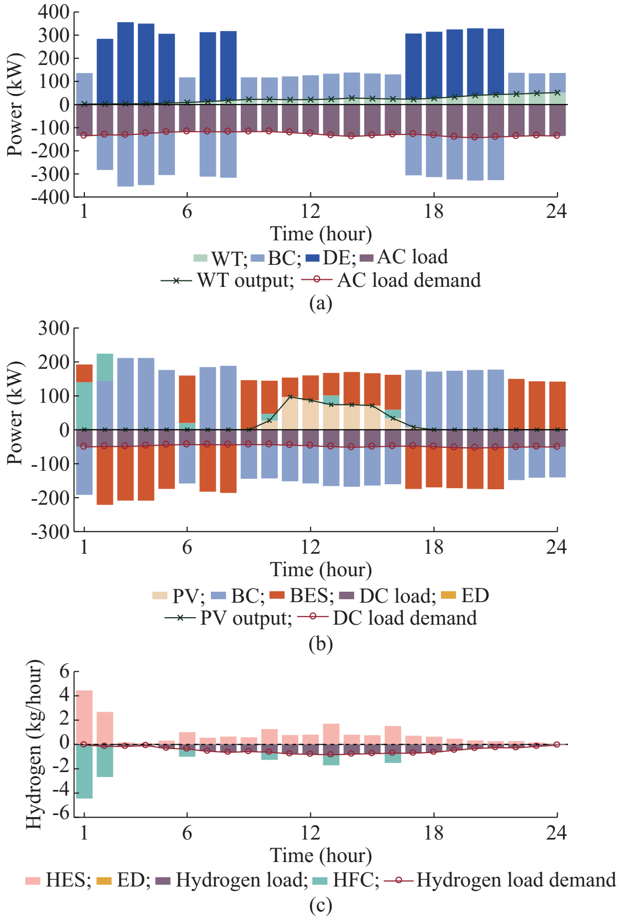

Fig. 7. Optimal results of daily day-ahead power dispatch on January 1 in case 2. (a) AC subsystem. (b) DC subsystem. (c) Hydrogen subsystem.

D. Optimal Results in Case 3

To further show the potential of the isolated electricity-hydrogen MG, the super-high penetration of RESs with 200 kW WT power and 1475 kW PV power is considered.

The optimal results of inter-day energy dispatch in case 3 are displayed in Fig. 8, and the optimization time is 3.228 s. Due to the isolated electricity-hydrogen MG deploying sufficient capacities of RESs and HES, one of the most apparent differences between case 2 and case 3 is that the DE does not need to participate in the annual scheduling plan. Due to the uncertainties, the isolated electricity-hydrogen MG still needs to deploy a DE to ensure the operational reliability.

To obtain the full-year dispatch performance of case 3, we perform the day-ahead power dispatch of case 3 for 365 days. The daily optimization time range is from 0.427 s to 61.003 s with an average of 3.604 s. The seasonal evaluation indicators for the isolated electricity-hydrogen MG in case 3 are as follows: the annual operating cost is \$240690.18, the annual green power ratio is 91.11%, the annual RESs utilization ratio is 98.54%, and the annual demand coverage ratio is 99.38%. This means that the seasonal mismatches associated with ultra-high penetration of RESs can be effectively addressed by utilizing hybrid electric-hydrogen energy storage. In particular, the optimal results of daily day-ahead power dispatch on January 1 in case 3 are shown in Fig. 9.

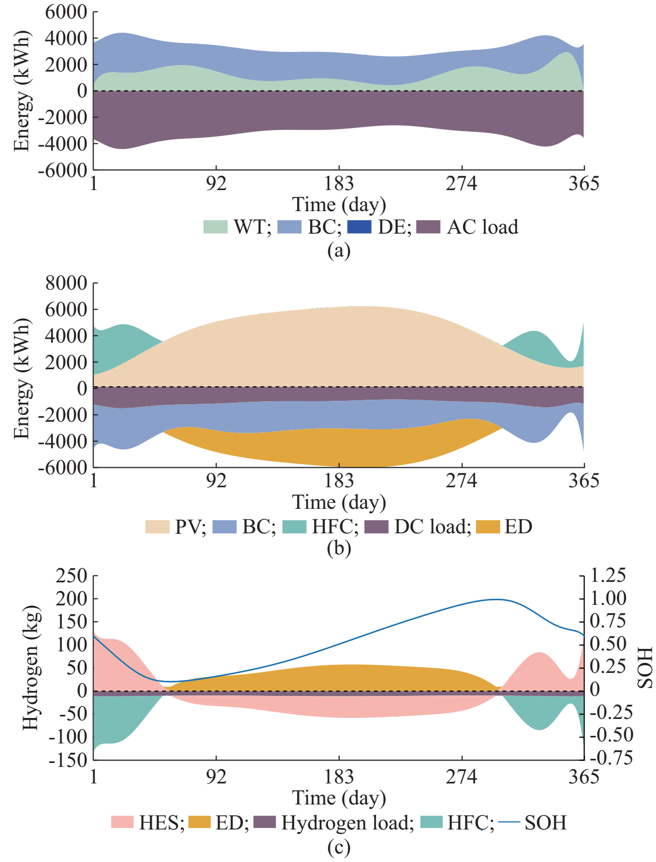

Fig. 8. Optimal results of inter-day energy dispatch in case 3. (a) AC subsystem. (b) DC subsystem. (c) Hydrogen subsystem.

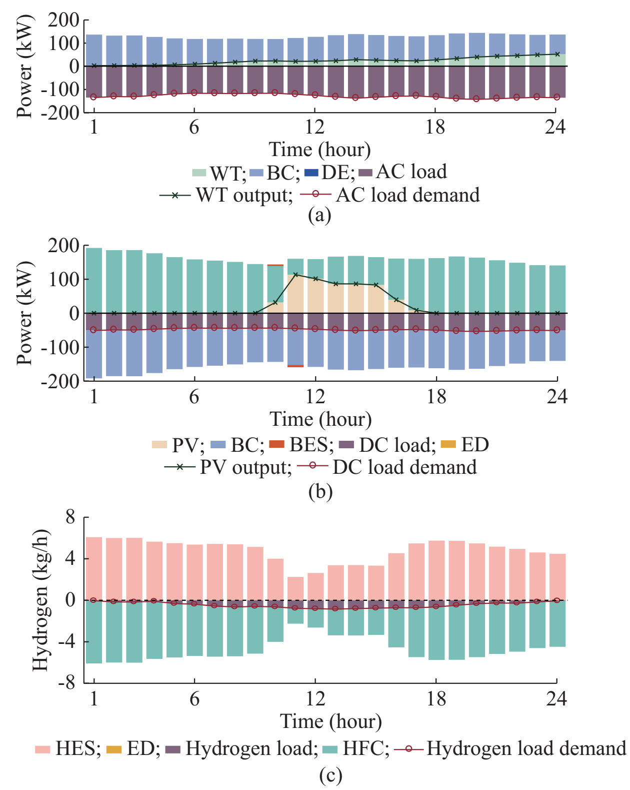

Fig. 9. Optimal results of daily day-ahead power dispatch on January 1 in case 3. (a) AC subsystem. (b) DC subsystem. (c) Hydrogen subsystem.

Table II lists the daily evaluation indicators of the day-ahead power dispatch on January 1 for three cases. We can find that the total daily operational cost of the isolated electricity-hydrogen MG in case 3 drops drastically.

TABLE II
DAILY EVALUATION INDICATORS OF DAY-AHEAD POWER DISPATCH ON JANUARY 1 FOR THREE CASES

Case	C_{day} (\$)	$R^{\text{daily}}_{\text{RESs,G}}$ (%)	$R^{\text{daily}}_{\text{RESs,U}}$ (%)	$R^{\text{daily}}_{\text{Load,S}}$ (%)
1	2070.25	20.20	100	96.85
2	1667.39	23.61	100	100.00
3	349.21	100.00	100	100.00

This is attributed to the significant increase in the green power ratio of case 3, and the outputs of renewable energy generation and hybrid battery-hydrogen energy storage meet the load demand on January 1. Thus, the use of DE is significantly reduced in case 3. Considering four cost factors, the operational cost of DE is expensive (in case 3, the cost of DE running at rated power is 0.3701 \$/h), resulting in a substantial reduction in the costs. It is worth noting that the daily evaluation indicators given here are calculated based on the results of the specified dates, which vary considerably from day to day.

Table III lists the seasonal evaluation indicators of isolated electricity-hydrogen MG. We can find that the annual operational cost of the isolated electricity-hydrogen MG drops significantly from case 1 to case 3.

TABLE III
SEASONAL EVALUATION INDICATORS OF ISOLATED ELECTRICITY-HYDROGEN MG

Case	C_{annual} (\$)	$R^{\text{annual}}_{\text{RESs,G}}$ (%)	$R^{\text{annual}}_{\text{RESs,U}}$ (%)	$R^{\text{annual}}_{\text{Load,S}}$ (%)
1	368780.55	68.23	73.23	98.41
2	276690.24	84.67	99.23	99.34
3	240690.18	91.11	98.54	99.38

The obtained results show that the isolated electricity-hydrogen MG and the proposed method are effective for the dispatch of isolated electricity-hydrogen MGs with super-high penetration of RESs. The green power ratio, RES utilization ratio, and demand coverage ratio are all improved with the implementation of the proposed method.

V. CONCLUSION

An effective way to solve the decarbonization problem of isolated electricity-hydrogen MGs is to increase the penetration of RESs. This paper presents an isolated electricity-hydrogen MG with AC subsystem, DC subsystem, and hydrogen subsystem. A specific hierarchical coordination optimization method is developed for the efficient operation of MG. An annual horizon is formulated as an inter-day energy dispatching model that aims to address seasonal energy mismatches. Considering the deviations between the estimated annual energy production and consumption data and the day-ahead forecast data, a hydrogen energy transmission chain is utilized to correct the end-of-day SOH. The day-ahead power dispatch is introduced to ensure the continuous power balance and economic operation of MG. Three cases with different penetrations of RES and different energy storage configurations are considered to prove the effectiveness of the proposed method. Simulation results show that the proposed method takes full advantage of hybrid battery-hydrogen energy storage to enable the energy saving and emission reduction of MG, reducing its dependence on DEs. It not only ensures the safe and economic operation of isolated electricity-hydrogen MGs with high penetration of RESs, but also regulates the current seasonal mismatch problem.

Further research on the forecast of energy production and consumption on long-time scales is planned. It is also worth conducting an in-depth study of the uncertainty of renewable energy output and load to maintain the safe operation of the MG. Meanwhile, the future work can also be extended to consider shorter time horizons to reduce the impact of day-ahead forecast errors.

REFERENCES

[1] L. Li, J. Wang, X. Zhong *et al*., "Combined multi-objective optimization and agent-based modeling for a 100% renewable island energy system considering power-to-gas technology and extreme weather conditions," *Applied Energy*, vol. 308, p. 118376, Feb. 2022.

[2] International Energy Agency. (2021, Dec.). Renewables 2021. [Online]. Available: https://www.iea.org/reports/renewables-2021

[3] Bruno Venditti. (2022, May). Mapped: solar and wind power by country. [Online]. Available: https://www.visualcapitalist.com/mapped-solar-and-wind-power-by-country/

[4] S. K. Panda and B. Subudhi, "A review on robust and adaptive control schemes for microgrid," *Journal of Modern Power Systems and Clean Energy*, vol. 11, no. 4, pp. 1027-1040, Jul. 2023.

[5] J. Zhu, S. Li, A. Borghetti *et al*., "Review of demand-side energy sharing and collective self-consumption schemes in future power systems," *iEnergy*, vol. 2, no. 2, pp. 119-132, Jun. 2023.

[6] B. Li, R. Roche, D. Paire *et al*., "Sizing of a stand-alone microgrid considering electric power, cooling/heating, hydrogen loads and hydrogen storage degradation," *Applied Energy*, vol. 205, pp. 1244-1259, Nov. 2017.

[7] J. Li, Z. Fang, Q. Wang *et al*., "Optimal operation with dynamic partitioning strategy for centralized shared energy storage station with integration of large-scale renewable energy," *Journal of Modern Power Systems and Clean Energy*, vol. 12, no. 2, pp. 359-370, Mar. 2024.

[8] CNESA. (2023, Jul.). Energy storage industry report. [Online]. Available: http://www.cnesa.org/information/detail/?column_id=3&id=5459

[9] P. Albertus, J. S. Manser, and S. Litzelman, "Long-duration electricity storage applications, economics, and technologies," *Joule*, vol. 4, no. 1, pp. 21-32, Jan. 2020.

[10] D. Pavković, M. Lobrović, M. Hrgetić *et al*., "A design of cascade control system and adaptive load compensator for battery/ultracapacitor hybrid energy storage-based direct current microgrid," *Energy Conversion and Management*, vol. 114, pp. 154-167, Apr. 2016.

[11] P. Colombo, A. Saeedmanesh, M. Santarelli *et al*., "Dynamic dispatch of solid oxide electrolysis system for high renewable energy penetration in a microgrid," *Energy Conversion and Management*, vol. 204, p. 112322, Jan. 2020.

[12] N. A. Sepulveda, J. D. Jenkins, A. Edington *et al*., "The design space for long-duration energy storage in decarbonized power systems," *Nature Energy*, vol. 6, no. 5, pp. 506-516, May 2021.

[13] O. Schmidt, S. Melchior, A. Hawkes *et al*., "Projecting the future levelized cost of electricity storage technologies," *Joule*, vol. 3, no. 1, pp. 81-100, Jan. 2019.

[14] L. Zhang and J. Xiang, "The performance of a grid-tied microgrid with hydrogen storage and a hydrogen fuel cell stack," *Energy Conversion and Management*, vol. 87, pp. 421-427, Nov. 2014.

[15] G. Cau, D. Cocco, M. Petrollese *et al*., "Energy management strategy based on short-term generation scheduling for a renewable microgrid using a hydrogen storage system," *Energy Conversion and Management*, vol. 87, pp. 820-831, Nov. 2014.

[16] X. Wang, W. Huang, N. Tai *et al*., "Two-stage full-data processing for microgrid planning with high penetrations of renewable energy sources," *IEEE Transactions on Sustainable Energy*, vol. 12, no. 4, pp. 2042-2052, Oct. 2021.

[17] Q. Sun, Z. Wu, W. Gu *et al*., "Multi-stage co-planning model for power distribution system and hydrogen energy system under uncertainties," *Journal of Modern Power Systems and Clean Energy*, vol. 11, no. 1, pp. 80-93, Jan. 2023.

[18] S. Li, J. Zhu, and H. Dong, "A novel energy sharing mechanism for smart microgrid," *IEEE Transactions on Smart Grid*, vol. 12, no. 6, pp. 5475-5478, Nov. 2021.

[19] J. Li, J. Lin, H. Zhang *et al*., "Optimal investment of electrolyzers and seasonal storages in hydrogen supply chains incorporated with renewable electric networks," *IEEE Transactions on Sustainable Energy*, vol. 11, no. 3, pp. 1773-1784, Jul. 2020.

[20] M. Tostado-Véliz, P. Arévalo, and F. Jurado, "A comprehensive electrical-gas-hydrogen microgrid model for energy management applications," *Energy Conversion and Management*, vol. 228, p. 113726, Jan. 2021.

[21] G. Pan, W. Gu, Y. Lu *et al*., "Optimal planning for electricity-hydrogen integrated energy system considering power to hydrogen and heat and seasonal storage," *IEEE Transactions on Sustainable Energy*, vol. 11, no. 4, pp. 2662-2676, Oct. 2020.

[22] X. Sun, X. Cao, M. Li *et al*., "Seasonal operation planning of hydrogen-enabled multi-energy microgrids through multistage stochastic programming," *Journal of Energy Storage*, vol. 85, p. 111125, Apr. 2024.

[23] R. Atia and N. Yamada, "Sizing and analysis of renewable energy and battery systems in residential microgrids," *IEEE Transactions on Smart Grid*, vol. 7, no. 3, pp. 1204-1213, May 2016.

[24] H. Qiu, W. Gu, Y. Xu *et al*., "Multi-time-scale rolling optimal dispatch for AC/DC hybrid microgrids with day-ahead distributionally robust scheduling," *IEEE Transactions on Sustainable Energy*, vol. 10, no. 4, pp. 1653-1663, Oct. 2019.

[25] Y. Du, J. Wu, S. Li *et al*., "Hierarchical coordination of two-time scale microgrids with supply-demand imbalance," *IEEE Transactions on Smart Grid*, vol. 11, no. 5, pp. 3726-3736, Sept. 2020.

[26] Z. Zhao, P. Yang, J. M. Guerrero *et al*., "Multiple-time-scales hierarchical frequency stability control strategy of medium-voltage isolated microgrid," *IEEE Transactions on Power Electronics*, vol. 31, no. 8, pp. 5974-5991, Aug. 2016.

[27] C. Ju, P. Wang, L. Goel *et al*., "A two-layer energy management system for microgrids with hybrid energy storage considering degradation costs," *IEEE Transactions on Smart Grid*, vol. 9, no. 6, pp. 6047-6057, Nov. 2018.

[28] S. Li, J. Zhu, H. Dong *et al*., "Multi-time-scale energy management of renewable microgrids considering grid-friendly interaction," *Applied Energy*, vol. 367, p. 123428, Aug. 2024.

[29] M. Farivar and S. H. Low, "Branch flow model: relaxations and convexification: part I," *IEEE Transactions on Power Systems*, vol. 28, no. 3, pp. 2554-2564, Aug. 2013.

[30] A. O. Rousis, I. Konstantelos, and G. Strbac, "A planning model for a hybrid AC-DC microgrid using a novel GA/AC OPF algorithm," *IEEE Transactions on Power Systems*, vol. 35, no. 1, pp. 227-237, Jan. 2020.

[31] B. R. Pereira, G. R. M. da Costa, J. Contreras *et al*., "Optimal distributed generation and reactive power allocation in electrical distribution systems," *IEEE Transactions on Sustainable Energy*, vol. 7, no. 3, pp. 975-984, Jul. 2016.

[32] R. Fang and Y. Liang, "Control strategy of electrolyzer in a wind-hydrogen system considering the constraints of switching times," *International Journal of Hydrogen Energy*, vol. 44, no. 46, pp. 25104-25111, Sept. 2019.

[33] L. P. Van, K. do Chi, and T. N. Duc, "Review of hydrogen technologies based microgrid: energy management systems, challenges and future recommendations," *International Journal of Hydrogen Energy*, vol. 48, no. 38, pp. 14127-14148, May 2023.

[34] Z. Abdin, A. Zafaranloo, A. Rafiee *et al*., "Hydrogen as an energy vector," *Renewable and Sustainable Energy Reviews*, vol. 120, p. 109620, Mar. 2020.

[35] B. Zhao, X. Zhang, J. Chen *et al*., "Operation optimization of standalone microgrids considering lifetime characteristics of battery energy storage system," *IEEE Transactions on Sustainable Energy*, vol. 4, no. 4, pp. 934-943, Oct. 2013.

[36] B. Zhao, H. Qiu, R. Qin *et al*., "Robust optimal dispatch of AC/DC hybrid microgrids considering generation and load uncertainties and energy storage loss," *IEEE Transactions on Power Systems*, vol. 33, no. 6, pp. 5945-5957, Nov. 2018.

[37] P. Veers, K. Dykes, E. Lantz *et al*., "Grand challenges in the science of wind energy," *Science*, vol. 366, no. 6464, p. eaau2027, Oct. 2019.

[38] A. Mansour-Saatloo, M. A. Mirzaei, B. Mohammadi-Ivatloo *et al*., "A risk-averse hybrid approach for optimal participation of power-to-hydrogen technology-based multi-energy microgrid in multi-energy markets," *Sustainable Cities and Society*, vol. 63, p. 102421, Dec. 2020.

[39] GAMS Development Corp. (2024, Dec.). General algebraic modeling system (GAMS) studio release 37. [Online]. Available: http://www.gams.com

[40] RTE. (2024, Dec.). Electric data of France's transmission system operator RTE. [Online]. Available: https://www. rte-france. com/eco2mix/telecharger-les-indicateurs

[41] Z. Deng and Y. Jiang, "Optimal sizing of wind-hydrogen system considering hydrogen demand and trading modes," *International Journal of Hydrogen Energy*, vol. 45, no. 20, pp. 11527-11537, Apr. 2020.

Jizhong Zhu received the B.S., M.S., and Ph.D. degrees in electrical engineering from Chongqing University, Chongqing, China, in 1985, 1987, and 1990, respectively. He is a Fellow of IEEE and a Professor at the School of Electric Power Engineering, South China University of Technology, Guangzhou, China. His research interests include power system operation and control, smart grid, microgrid, virtual power plant, electric vehicle, renewable energy application, and integrated smart energy system.

Taiheng Guo received the B.S. and M.S. degrees from South China University of Technology, Guangzhou, China, in 2020 and 2025, respectively. He is currently working in Electric Power Research Institute of Guangdong Power Grid Co., Ltd., Guangzhou, China. His current research interests include renewable energy consumption and microgrid energy management.

Shenglin Li received the B.S. and M.S. degrees from Shanghai University of Electric Power, Shanghai, China, in 2016 and 2019, respectively, and the Ph.D. degree in electrical engineering from South China University of Technology, Guangzhou, China, in 2023. He is currently working as a Postdoctoral Fellow in South China University of Technology. His research interests include demand-side energy management, and optimal dispatch in microgrid and distribution network.

Hanjiang Dong received the B.S. degree in electrical engineering and its automation from Jinan University, Guangzhou, China, in 2020. He is currently working toward the joint Ph.D. degree with the School of Electric Power Engineering, South China University of Technology, Guangzhou, China, and the Department of Electrical and Electronic Engineering, The Hong Kong Polytechnic University, Hong Kong, China. His current research interests include power system operation, load forecasting, energy economic, and microgrid.

Alberto Borghetti graduated in electrical engineering from the University of Bologna, Bologna, Italy, in 1992. Since he has been working with the Power System Group, University of Bologna, where he is now a Professor of electrical power systems. He is serving as an Associate Editor of Modern Power Systems and Clean Energy (MPCE). His research interests include power system analysis, power system restoration after blackout, electromagnetic transients, optimal generation scheduling, and distribution system operation.

Xuemeng Lan received the B.S. degree from South China University of Technology, Guangzhou, China, in 2024. She is currently pursuing the M.S. degree with the School of Electric Power Engineering, South China University of Technology. Her research interest is optimization of power system emergency control.